Available online at www.sciencedirect.com
SCIENCE DIRECT®

Journal of the European Ceramic Society 23 (2003) 3135–3146
www.elsevier.com/locate/jeurceramsoc

Influence of long term oxidation on the microstructure, mechanical and electrical properties of pressureless sintered AlN–SiC–$MoSi_2$ ceramic composites

Kristoffer Krnel*[,1], Diletta Sciti, Alida Bellosi

CNR-ISTEC, Institute of Science and Technology for Ceramics, Via Granarolo 64, I-48018 Faenza, Italy

Received 28 July 2002; received in revised form 27 January 2003; accepted 8 February 2003

Abstract

The effects of long term oxidation on the microstructural modification and on the electrical resistivity and mechanical strength of an AlN–SiC–$MoSi_2$ electroconductive ceramic composite are presented. The microstructure of the pressureless sintered composite is described and the oxidation behaviour is discussed. The formation of protective mullite layer at temperatures above 1000 °C provides good oxidation resistance for use at higher temperatures. At temperatures below 1000 °C, the AlN/SiC matrix disables the ''pesting'' phenomena and strength degradation, despite the fact that at these temperatures $MoSi_2$ oxidizes rapidly. The surface modification induced by oxidation on AlN–SiC–$MoSi_2$ composites does not affect the mechanical strength, while the electrical conductivity strongly decreases.

Keywords: AlN–SiC–$MoSi_2$; Composites; Corrosion; Electrical properties; Mechanical properties; Microstructure-final

1. Introduction

New ceramic materials attract the scientific community as well as industries, because of their outstanding combination of physical and chemical properties for use at high temperatures and in an aggressive environment.[1] Wear and corrosion resistant, chemically inert and electrical conductive ceramics are interesting materials for applications where electrically conductive components or small precision parts with complex geometry are applied. The development of structural electrically conductive ceramic is not simple, namely conductive ceramic materials are usually brittle and do not sinter well, and on the other side, engineering ceramic materials are insulators. A promising approach is a combination of insulating engineering ceramics with electrically conductive phases.[2]

Among the electrically conductive ceramics, $MoSi_2$ has a combination of properties suitable for several high temperature applications; in fact the formation of a protective silica layer at temperatures above 1000 °C provides good oxidation resistance for use at higher temperatures. Its deficiencies are low ductility at temperatures below 1000°, poor strength and creep resistance at temperatures above 1250 °C, and the so-called pesting in which disintegration occurs at temperatures from 500 to 800 °C.[3]

To avoid these problems, the best approach is to prepare ceramic composites using matrix materials with good mechanical properties and oxidation resistance. Recently, composites of $MoSi_2$ with SiC showed an improvement of strength, toughness and oxidation resistance compared to monolithic $MoSi_2$.[4–6]

The present paper focuses on the effects of long term oxidation in air, in the temperature range 600–1400 °C, on the microstructural modification and on the behaviour of electrical resistivity and mechanical strength at room temperature of an AlN–SiC–$MoSi_2$ composite. This material is a possible candidate for electroconductive engineering material for use as igniters, heaters or parts of turbines and automobile engines, with

* Corresponding author. Tel.: +386-14773784; fax: +386-14263126.
E-mail address: kristof.krnel@ijs.si (K. Krnel).
[1] Present address: Jožef Stefan Institute, Jamova 39, 1000 Ljubljana, Slovenia

0955-2219/03/$ - see front matter © 2003 Elsevier Ltd. All rights reserved.
doi:10.1016/S0955-2219(03)00095-5

possible on-line damage and oxidation control due to its electrical conductivity.

2. Experimental procedure

The powders used for the preparation of composite material are as follows: AlN Grade C powder (H.C. Starck, Berlin, Germany) with d_{50} 2.29 μm, oxygen content of 1.8% and specific surface area of 4.3 m^2/g; SiC BF-12 (H.C. Starck, Berlin, Germany) with 97% of β-SiC, mean particle size 0.23 μm, oxygen content of 0.88% and specific surface area of 8.12 m^2/g; $MoSi_2$ (Aldrich, Milwaukee, USA) with mean particle size 2.8 μm and oxygen content of about 1%; Y_2O_3 grade C (H.C. Starck, Berlin, Germany) was used as a sintering aid.

The following composition: 55 vol.% AlN + 15 vol.% SiC + 30 vol.% $MoSi_2$, to which 2 wt.% of Y_2O_3 was added as a sintering aid, was selected on the basis of preliminary experiments. The powder mixture was prepared by ball milling for 24 h in absolute ethanol using silicon nitride balls. The slurry was dried in a rotary evaporator and sieved. Sample bars with green dimensions 4×5×30 mm were prepared by uniaxial pressing followed by cold isostatic pressing under 350 MPa. Bars were pressureless sintered in AlN/BN powder bed at 1900 °C for 1 h in flowing nitrogen. Sintered densities were measured using Archimedes method.

Samples were then oxidised in batches of five at 600, 800, 1200, 1300 and 1400 °C for 100 h in laboratory air. The weight gain $\Delta w/S$ (mg/cm^2) was evaluated on all the samples after the oxidation tests. Oxidised and as-sintered sample surfaces were analysed with X-ray diffraction.

Sample surfaces, polished cross sections and fracture surfaces were analyzed by scanning electron microscopy and energy dispersive microanalysis (SEM–EDX).

Fracture strength of as-sintered and oxidised samples were measured using four point bending jig with a lower span 20 mm and upper span 10 mm on an universal screw-type testing machine Instron 1195 (Instron, USA) with a crosshead speed of 0.05 mm/min. Five bars were tested for each oxidation temperature.

Electrical resistivity of as-sintered samples was measured using the four probe DC method at room temperature inducing a longitudinal current along the bar. The current and the voltage were detected at the same time with high-resolution multimeters. The resistivity value was determined from the electrical resistance taking into account the test leads distance and cross section area of the sample. On the oxidised samples the above described method is not applicable, since the oxide on the surface is a good insulator. Therefore, electrical resistivity was determined by measurements of resistance in a resistivity cell (HP 16008A, Hewlett-Packard, USA) in conjunction with a high resistance meter (HP 4392A, Hewlett-Packard, USA). To assure good and uniform electrical contact, the specimens were placed in a chamber with two highly conductive rubber electrodes between sample and metal electrode. All the measurements were made at various voltages from 10 to 500 V.

3. Results and discussion

3.1. Microstructure of the starting material

There is not much porosity present in the sintered AlN/SiC/$MoSi_2$ composites, as visible from Fig. 1(a and b), the relative density is 99.4% of the theoretical density.

Crystalline phases determined by XRD analysis are shown in Fig. 3: tetragonal $MoSi_2$, hexagonal AlN, $Y_3Al_5O_{12}$ (YAG), $Mo_{4.8}Si_3C_{0.6}$ (Nowotny phase), Mo_5Si_3, hexagonal 2H SiC and MoB. This last phase, present on the surface of the as sintered sample, is probably due to presence of BN in the powder bed used during sintering.

The microstructure of a polished surface, presented in Figs. 1 and 2, reveals bright particles that correspond to molybdenum disilicide (EDX analysis, Fig. 2, point 1), whereas the dark phase is composed of AlN and SiC, which are not distinguishable (EDX analysis, Fig. 2, point 4). EDX analysis of AlN grains also shows a small amount of Si present. The dark-phase grains are surrounded by a brighter grey grain boundary phase, formed from the liquid phase during sintering, due to the reaction among the added Y_2O_3 and alumina and silica from the oxidised surfaces of AlN and SiC powders, respectively. The composition of the grain boundary phase is close to the YAG phase ($Al_5Y_3O_{12}$), with excess of yttria (EDX analysis, Fig. 2, point 2), however the presence of glassy yttrium silicates cannot be excluded. There are no cracks visible between $MoSi_2$ and the matrix phase in spite of quite different thermal expansion coefficients of the present phases, which indicates good adhesion among the grains of different composition. Some $MoSi_2$ grains (an example is shown in Fig. 2) contain areas, appearing with two different grey levels that correspond to different stoichiometries. The content of Mo present in the brighter part is higher than in the less bright part: the ratio between Mo and Si peaks height of the EDX spectra is close to that of Mo_5Si_3 and/or $Mo_{4.8}Si_3C_{0.6}$, confirming the results of the XRD analyses. Detailed quantitative analysis of these phases was not performed, because the phase composition was already revealed by the XRD analysis. The presence of $Mo_{4.8}Si_3C_{0.6}$ in $MoSi_2$/SiC composites was already described by Niihara et al.[7] The EDX analysis of $MoSi_2$ grains (EDX analysis, Fig. 2, point 1) reveals also a small amount of Al.

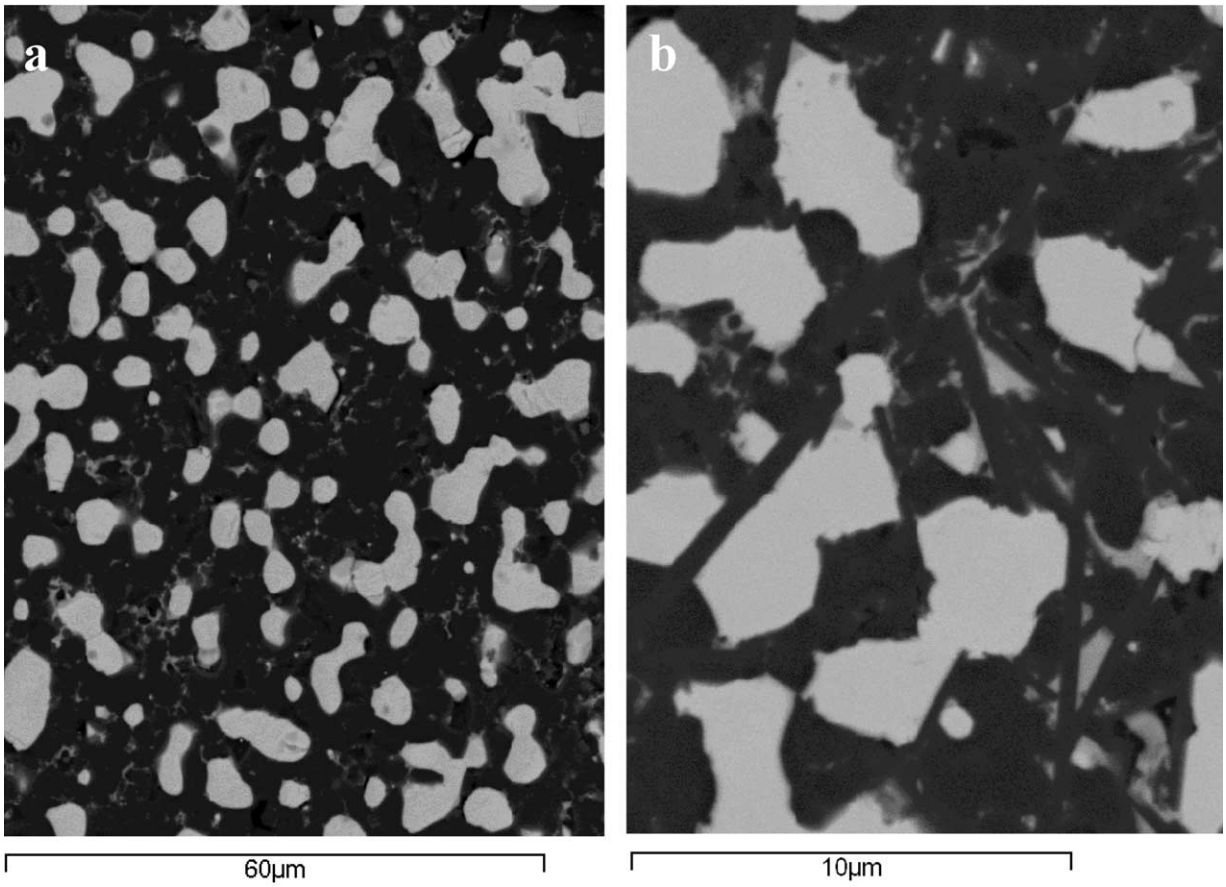

Fig. 1. BSE images of polished as sintered AlN/SiC/$MoSi_2$ composite.

It is well known that at temperatures $\geqslant$1900 °C, β-SiC phase undergoes the β→α transition, transforming into hexagonal SiC polytypes. In the present material, after sintering, only hexagonal 2H SiC was detected and this phase can form solid solutions with hexagonal AlN, due to their matching lattice parameters. As a matter of fact, some elongated AlN grains were observed on SEM micrograph (Fig. 1b), inside which Si was detected using EDX microanalysis. This supports the hypothesis of solid solution formation, since the elongated grains grew from liquid phase present during sintering. These elongated grains could also be the SiAlON phase, but their amount was to high and also no oxygen signal was detected on the EDX spectra. In contrast, the phase conversion β-SiC→2H-SiC was not observed when this material was prepared by hot pressing, most probably because of lower sintering temperature (1800 °C). Using hot pressing these solid solutions were observed at temperatures exceeding 2000 °C.[8] These results also confirm that the temperature necessary for the formation of AlN–SiC solid solution is above 1900 °C.[9]

3.2. Characterisation of the oxidation product

The dependence of weight change on the oxidation temperature, presented in Fig. 4a, reveals that the samples oxidized at 600 and 800 °C lose weight, whereas at oxidation temperatures above 1000 °C they gain weight. The thickness of the oxidised layer, measured on SEM micrographs of the polished sample cross-sections, increases with increasing oxidation temperature (Fig. 4b).

The XRD spectra of surfaces of oxidised samples are shown in Fig. 3 along with the spectrum of the surface of the as sintered sample. The patterns of the samples oxidized at 600 and 800 °C do not differ much from the spectra of the sintered material. The intensity of $Mo_{4.8}Si3C_{0.6}$ and MoB peaks is lower in the spectra of the sample oxidised at 600 °C compared to the as-sintered material and these phases are absent in the surface of the sample oxidised at 800 °C, probably due to their complete decomposition to volatile molybdenum oxides in a subsurface layer of the composite, as discussed below.

XRD patterns of the sample oxidized at 1200 °C show the presence of $MoSi_2$, AlN, mullite, Mo_5Si_3 and traces of α-Al_2O_3. Although $MoSi_2$, AlN and Mo_5Si_3 are still detectable among the surface crystalline phases in the sample oxidized at 1300 °C, mullite and alumina are even more evident. After thermal treatment at 1400 °C only mullite peaks are visible.

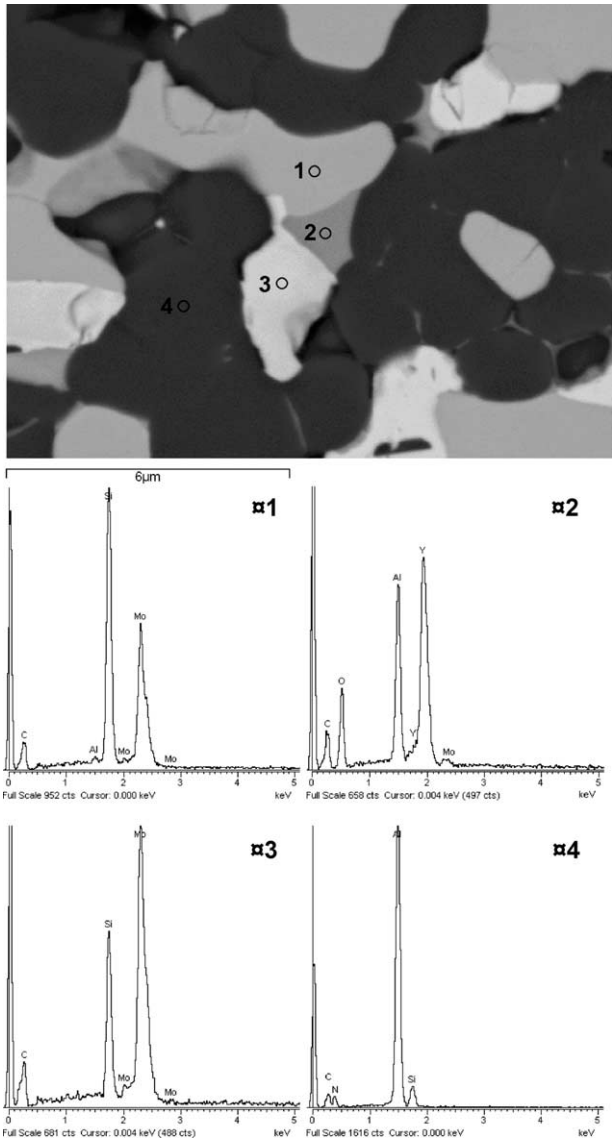

Fig. 2. BSE image and EDX phase analysis of polished as sintered AlN/SiC/$MoSi_2$ composite.

The surfaces and the cross sections of as sintered and oxidised samples are shown in Figs. 5a–f and 6a–f, respectively.

On the surface of the sample oxidized at 600 and 800 °C small grains of a new phase formed, which is most probably amorphous silica derived from the oxidation of molybdenum silicide. The cross section morphology evidences that the treatment at 800 °C induced a degradation of the material in the subsurface layer (Fig. 6c). Pores and cracks, present up to a depth of about 100 μm from the external surface, were formed as a consequence of the oxidation of molybdenum disilicides and of molybdenum boride to gaseous species that escaped through interconnected voids.[10] Defects and voids are responsible for the propagation of oxidation towards the bulk of the samples.

The surface of the sample oxidized at 1200 °C (Fig. 5d) is similar to those oxidised at 600 and 800 °C. Small grains of a newly formed phase are also visible. These are probably mullite grains resulting from reaction between silica and alumina formed by the oxidation of $MoSi_2$, SiC and AlN.

The analysis of the cross section (Fig. 6d) reveals that the mullite layer is very thin and beneath it Mo_5Si_3 inclusions are present, as confirmed by X-ray diffraction. This phase is still detectable after oxidation at 1200 °C due the fact that the mullite layer is relatively thin and Mo_5Si_3 scattering factor is much higher than the scattering factor of mullite. There are also some pores visible next to the reaction interface, due to the initial partial elimination of molybdenum-containing particles, as discussed below.

The surface of the samples oxidized at 1300 and 1400 °C (Fig. 5e and f) is completely covered with a network of mullite crystals interconnected with glassy silica. On the cross section (Fig. 6e and f) no other intermediate phase was observed between mullite oxide layer and bulk composite material, besides Mo_5Si_3 present in the bulk next to the reaction interface (white grains, connected to bright $MoSi_2$ grains). The thickness of the oxidation products is 20 μm after treatment at 1300 °C and more than 50 μm at 1400 °C.

3.3. Oxidation behaviour

The long term (100 h) oxidation test in air at temperatures between 600 and 1400 °C induced a surface and subsurface modification that involved both the oxidation of the phases present in the AlN/SIC/$MoSi_2$ composite and the reaction among the oxidation products. It is well known that AlN and SiC have very high resistance to oxidation thanks to the development of a protective oxide scale of alumina and silica, respectively.[11]

In contrast, the oxidation behaviour of Mo-based silicides has been intensively investigated, because this material has an excellent oxidation resistance at temperatures above 1000 °C, but undergoes rapid oxidation with consequent disintegration at temperatures between 500 and 800 °C. It is generally recognised that, depending on exposure conditions, two competitive phenomena occur: the growth of silica and formation of Mo oxide and its volatilization.[12–16] The possible reaction is the following:

$$MoSi_2(s) + 3.5O_2(g) \rightarrow MoO_3(s) + 2SiO_2(s) \quad (1)$$

MoO_3 has a high vapour pressure which makes it volatile between 500 and 800 °C and it melts at 795 °C. Thus, at low temperatures, the oxidation process is dominated by the formation of MoO_3, since the formation of SiO_2 is not fast enough. Very high internal stresses arise at the grain boundaries, due to volume

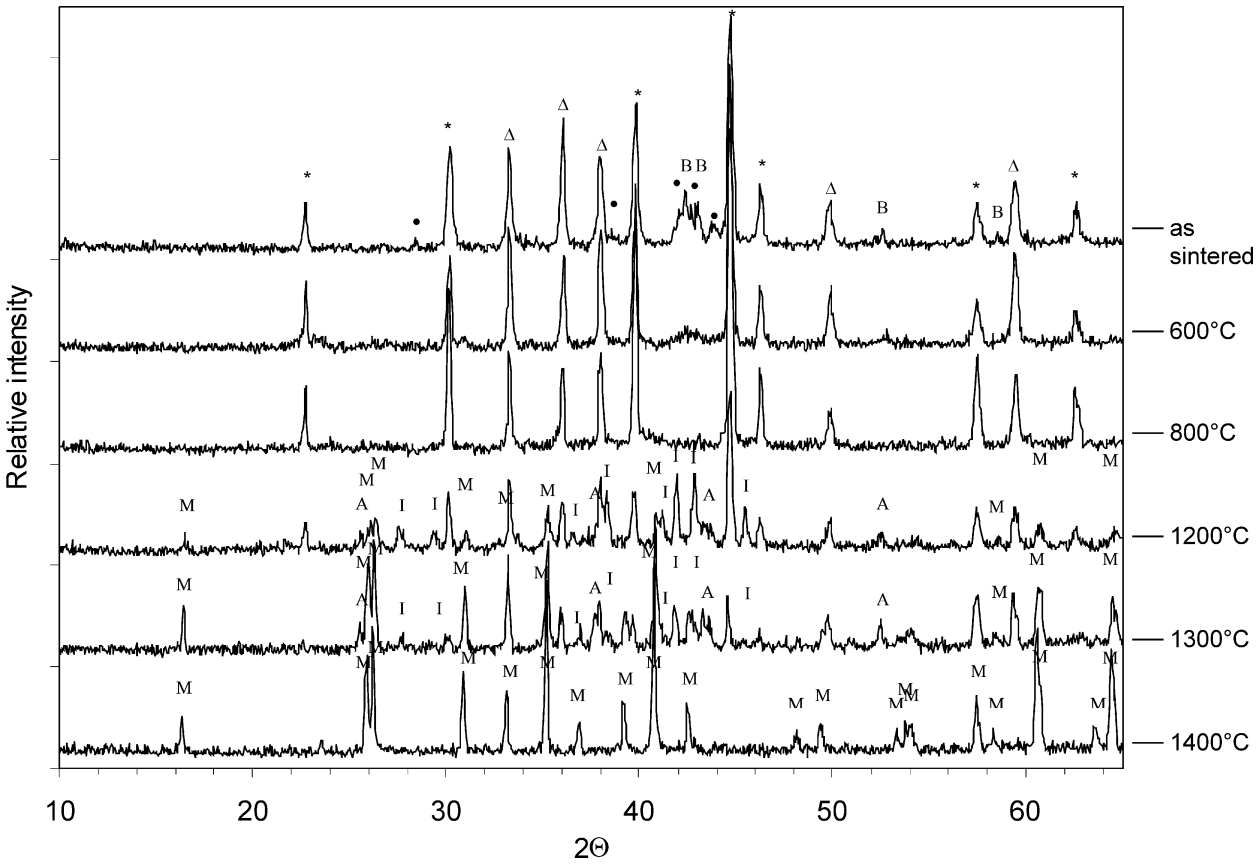

Fig. 3. XRD analysis of the surface of as sintered and oxidised samples (*—$MoSi_2$; D—AlN; ·—$Mo_{4.8}Si_3C_{0.6}$; B—MoB; I—Mo_5Si_3; A—Al_2O_3; M—mullite).

expansion caused by MoO_3 formation and to internal pressure build-up caused by MoO_3 volatilization. This can result in severe pesting.

At intermediate temperatures, SiO_2 forms slowly and generally it does not fully protect the material, such that MoO_3 continues to form and to evaporate. At $T > 1000\,^{\circ}C$, a rather continuous SiO_2 scale forms and seals the surface, preventing the bulk from further oxidation.

The reaction of $MoSi_2$ with oxygen involves also the formation of Mo_5Si_3 as intermediate product, in addition to silica. According to thermodynamic calculations carried out by Zhu et al. at temperatures above 800 °C, the oxidation of $MoSi_2$ to Mo_5Si_3 can be expressed as:[13]

$$5MoSi_2(s) + 7O_2(g) \rightarrow Mo_5Si_3(s) + 7SiO_2(s) \quad (2)$$

In particular at 1000 °C, the formation of Mo_5Si_3 is more favoured than formation of MoO_3. Mo_5Si_3 can further oxidise to MoO_3:

$$Mo_5Si_3(s) + 10.5\ O_2(g) \rightarrow 5\ MoO_3(g) + 3\ SiO_2(s) \quad (3)$$

Therefore, the phenomena occurring during the oxidation cycles of the composite are strongly related to the oxidation temperature. At low temperatures, oxidation is dominated by evaporation of MoO_3 formed by oxidation of $MoSi_2$ (according to reaction 1) and of $Mo_{4.8}Si_3C_{0.6}$, also present in the sample. The surface formation of glassy silica and probably some amorphous alumina is not efficient in protecting the samples. The net result is a slight weight loss. In spite of the absence of the protective layer, a severe material degradation did not occur. In fact, as reported in the Section 3.4, fracture strength did not vary significantly compared to the as-sintered sample. Recent research on the oxidation of Mo silicides has shown that the addition of elements such as Al, Ta, Ti, Zr, or Y, form oxides that are more stable than SiO_2 and accelerate the scaling process.[15] Al in particular, reduces pesting by formation of an amorphous Mo–Si–Al–O phase in the initial cracks and voids. Other works on $Mo(Al,Si)_2$ ceramics pointed out that even very small amounts of Al present in the $MoSi_2$ lattice can prevent these material from pesting.[17] In our case, being the matrix material an AlN–SiC composite, it is very likely that Al can be incorporated into the $MoSi_2$ lattice, preventing it from pesting, which was also confirmed by EDS analysis of $MoSi_2$ grains (Fig. 2).

In addition, accelerated oxidation and pesting are strongly affected by pre-existing defects and pores loca-

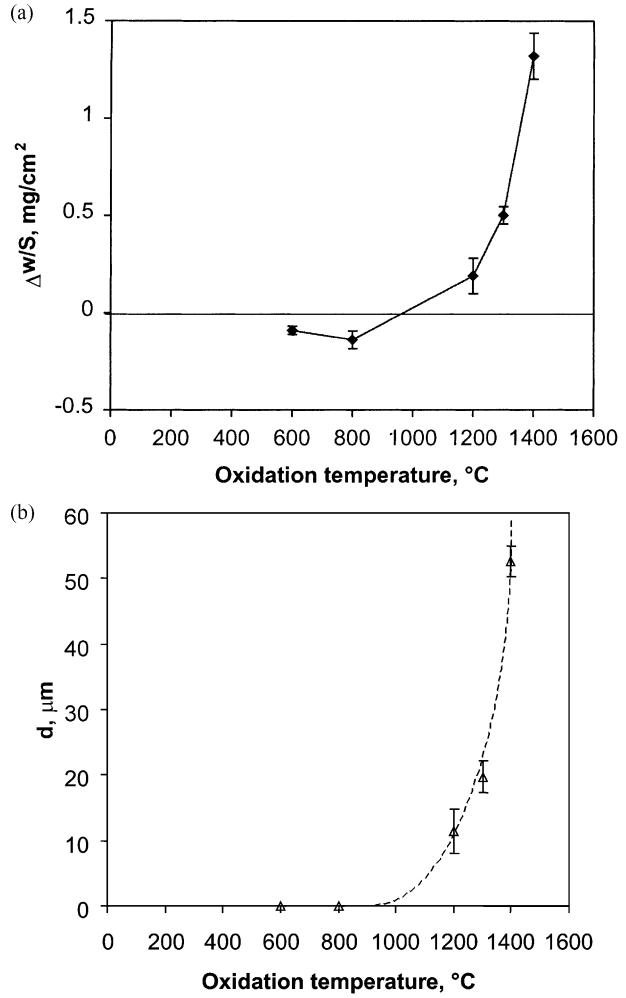

Fig. 4. Relative weight change (a) and thickness of oxidised layer (b) versus oxidation temperature.

ted at the surface of $MoSi_2$, but it was found[10] that pesting is completely suppressed in $MoSi_2$ with a theoretical density of > 99%. In the composite of the present study, the reasons for good resistance to pesting are either the high density of the as-sintered material or the presence of the AlN/SiC matrix, as main phase, that does not oxidise massively and good adhesion among the phases. All these factors contribute to prevent the material from disintegration during oxidation at temperatures in the range 600–800 °C.

In the range 1200–1400 °C $MoSi_2$ oxidation, reaction (1) becomes competitive with oxide scale formed by the oxidation of AlN and SiC. Therefore, from AlN oxidation, both alumina and $Al_{10}N_8O_2$ can form, which further reacts with silica, forming mullite. The possible reactions are:[18]

$$3\ Al_2O_3 + 2\ SiO_2 \rightarrow 3\ Al_2O_3.2\ SiO_2 \quad (4)$$

and

$$0.6\ Al_{10}N_8O_2 + 2\ SiO_2 + 3.9\ O_2 \rightarrow 3\ Al_2O_3.2\ SiO_2 + 2.4\ N_2 \quad (5)$$

Other possibility is the formation of SiAlON-s as a result of oxidation of AlN–SiC solid solution, according to the reaction:[18]

$$\left[(SiC_{1-x})(AlN)_x\right] \rightarrow Si_{6-z}Al_zO_zN_{8-z} + SiO_2 + CO + N_2 \quad (6)$$

In the XRD patterns, crystalline alumina was detected, but $Al_{10}N_8O_2$ or SiAlON-s phase were not observed on our spectra. However this does not exclude the possibility of their formation, since the detectability of XRD is in the order of 1% and their concentration can be below this limit. Their presence were confirmed in previous studies on oxidation of AlN–SiC composites with composition similar to the matrix of the present material.[18] Ramberg et al.,[17] on the other hand, showed that mullite does not form by solid-state reaction of discrete alumina and silica but is rather formed in situ during oxidation, which can also be the case here.

Simultaneously, at these temperatures, $MoSi_2$ oxidation proceeds with the formation of Mo_5Si_3, according to reaction (2) as intermediate product, as revealed by the cross section analysis. However, further oxidation of $MoSi_2$ and Mo_5Si_3 to MoO_3, reaction (3), is prevented by the presence of mullite protective layer, which hinders oxygen diffusion. At 1200° C the pores visible next to the reaction interface (Fig. 6d) are due to a partial elimination of molybdenum containing particles which occurs, since the mullite layer is not completely formed. The net result is a slight weight gain. In materials treated at 1300 and 1400 °C, no more pores are present and the weight gain increases as a result of the mullite layer thickness increases. The protective nature of the mullite scale was confirmed in our previous studies by TG analysis carried out on similar materials produced by hot pressing, which show that the oxidation kinetics in these materials is parabolic in the 1200–1400 °C range.

Finally, the presence of Y_2O_3 as sintering aid in the starting material does not seem to influence the oxidation behaviour. The YAG phase peaks, detected by X-ray in the as sintered samples, where not longer found after oxidation cycles, due to the presence of the oxide scale. On the other hand, previous studies on AlN oxidation behaviour up to 1390 °C, confirmed that pure AlN and Y_2O_3 doped AlN have almost the same behaviour in terms of oxidation kinetics and oxidation products.[11]

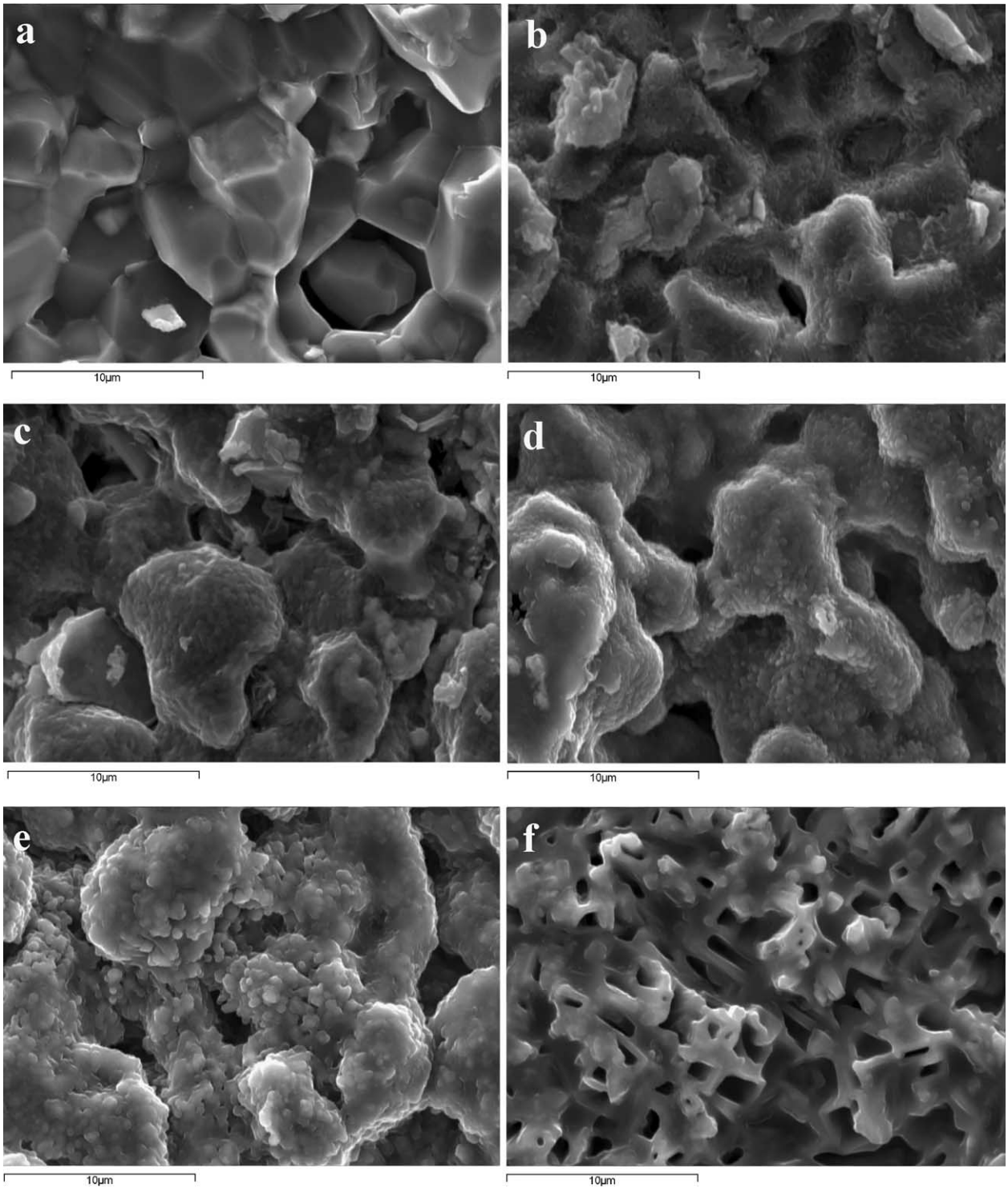

Fig. 5. Surfaces of as sintered and oxidised samples: (a) as sintered; (b) 600 °C, 100 h; (c) 800 °C, 100 h; (d) 1200 °C, 100 h; (e) 1300 °C, 100 h; (f) 1400 °C, 100 h.

3.4. Fracture strength

The fracture strength values for samples oxidised at various temperatures are presented in Fig. 7. The strength of non-oxidised samples is comparable with the values obtained for presureless sintered matrix material (AlN–SiC).[19] The changes in strength after oxidation are small and all within the standard deviation. The oxidation does not seem to have detrimental effect on the strength of this material.

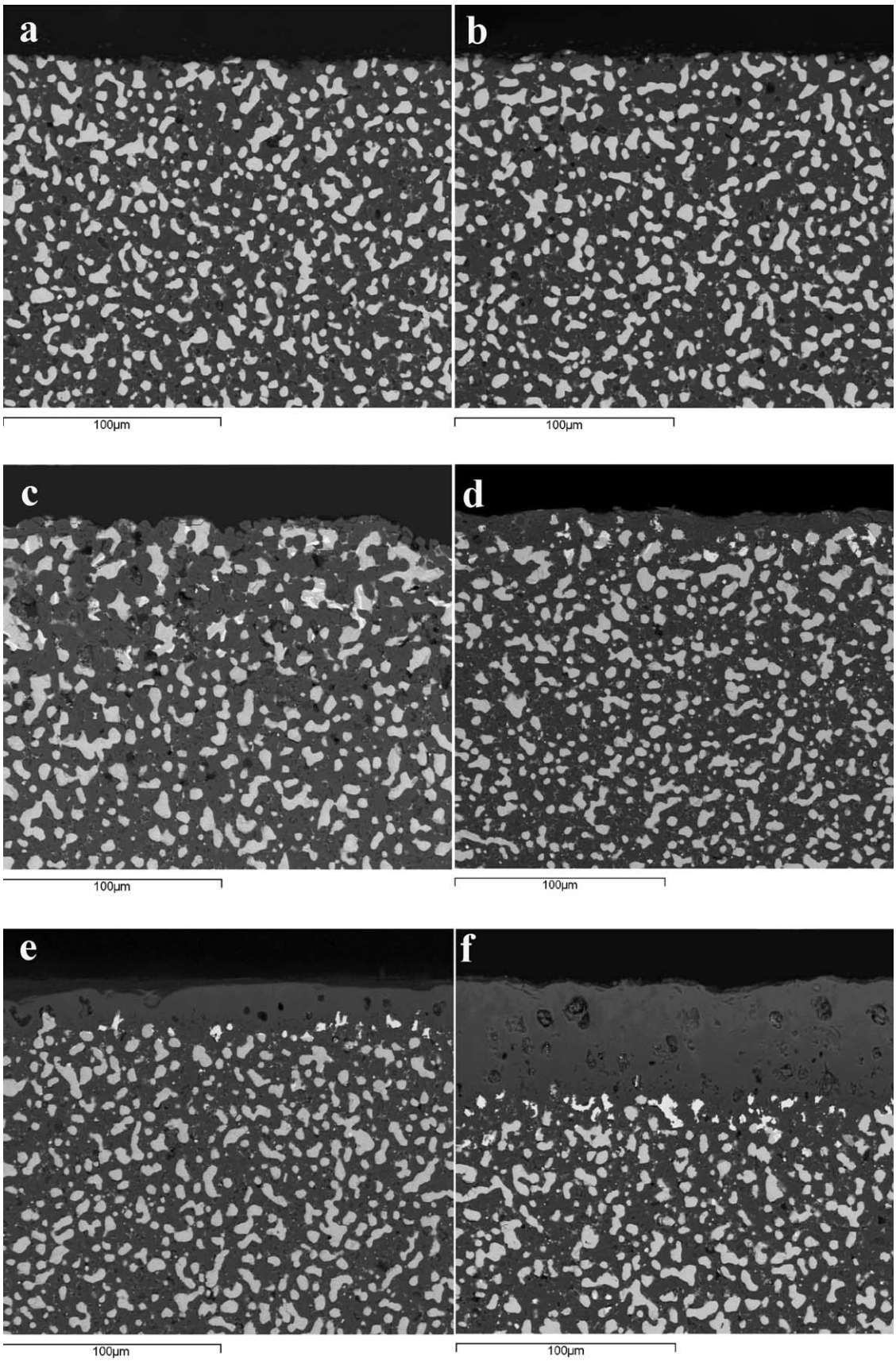

Fig. 6. Cross sections of as sintered and oxidised samples: (a) as sintered; (b) 600 °C, 100 h; (c) 800 °C, 100 h; (d) 1200 °C, 100 h; (e) 1300 °C, 100 h; (f) 1400 °C, 100 h.

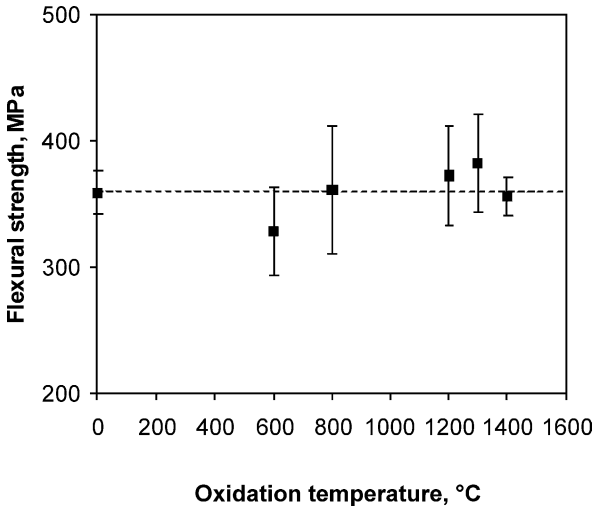

Fig. 7. Fracture strength of as sintered samples and samples oxidised at various temperatures for 100 h.

A little lower strength value at 600 °C can result from evaporation of MoO_3 from the surface voids due to limited oxidation of $MoSi_2$ particles.[20] At this temperature the oxidation is not fast enough to form a protective layer of mullite. Notwithstanding the subsurface porosity observed in the samples oxidized at 800 °C, their strength is similar to the starting material value. At higher temperatures the thin layer of mullite formed on the surface inhibits the oxidation of $MoSi_2$ and thus the formation of voids. The massive amount of mullite detected in samples oxidised at 1200 and 1300 °C can also be the reason for a little strength improvement, due to a partial sealing of pre-existing surface critical defects.[21] At 1400 °C however, the oxidation is much faster and already starts to influence the strength of the samples, which is, nevertheless still in the starting material range. From the fracture analysis, there was no evidence of fracture origin defects specifically attributable to oxidation. As an example, in the fracture surfaces of sample oxidised at 1300 °C (Fig. 8) the fracture originated from a crack on the surface, which does not look to be the consequence of oxidation but rather of sample preparation.

The results of the strength behaviour highlight the suitability of this electroconductive structural ceramic to be applied at working temperatures in the range 1000–1400 °C, without degradation of this property. Attention has to be addressed when these materials are applied under oxidizing environments in the temperature range 500–1000 °C, unless a preliminary treatment is performed at 1200–1300 °C in order to develop a surface protective oxide scale.

3.5. Electrical resistivity

The results of electrical resistivity measurements, presented in Figs. 9 and 10, show that the resistivity increases with the oxidation temperature. Even at oxidation temperature of 600 °C, the electrical resistivity is much higher (about 7 orders of magnitude) than that of as sintered sample, which is 2.5×10^{-3} Ωcm. This was expected on the basis of partial decomposition and volatilisation of the electrically conductive phase ($MoSi_2$). However, the measurement made on the samples oxidised at 600 and 800 °C are very unstable due the non-homogeneous surface morphology and composition (Fig. 11a); the reported results represent the mean value of several measurements. At higher temperatures of oxidation (1300 and 1400 °C), the measurement are stable and well repetitive, even at higher voltages, as can be seen from Fig. 10. The plot in Fig. 10 indicates that the increase of the electrical resistivity approaches asymptotically a value of $\sim10^{11}$ Ωcm, not very far from the resistivity of pure mullite ($\sim10^{13}$ Ωcm).[22] In fact, the oxide layer developed during the thermal treatment at 1400 °C is rather uniform (Fig. 11b) and thick enough to mask the influence of the conductive bulk material.

The results point out that the application of this composite in oxidising environment involves a strong decrease of the electrical conductivity and it has to be carefully considered when the electrical function is of leading importance. The material starts as electroconductive and rapidly becomes electrical insulator on the surface.

4. Conclusions

The AlN–SiC–$MoSi_2$ composite material pressureless sintered at 1900 °C for 1 h is dense, with theoretical density of 99.4%. Phases detected in the as sintered sample are: tetragonal $MoSi_2$, hexagonal AlN, β-SiC, $Y_3Al_5O_{12}$ (YAG), $Mo_{4.8}Si_3C_{0.6}$, Mo_5Si_3 and 2H SiC and MoB. After the oxidation at temperatures below 1000 °C, samples lose weight, due to evaporation of MoO_3 formed by the oxidation of $MoSi_2$, whereas at temperatures above 1000 °C they gain weight due to protective mullite layer formation on the surface. The results of the strength behaviour indicate the application of this electroconductive structural ceramic at temperatures in the range 1000–1400 °C, without degradation of this property. There was no strength degradation even at lower temperatures, but modification of the surface layer was observed. So when these materials are to be applied under oxidizing environments in the temperature range 500–1000 °C a preliminary treatment should be performed at 1200–1300 °C in order to develop a surface protective oxide

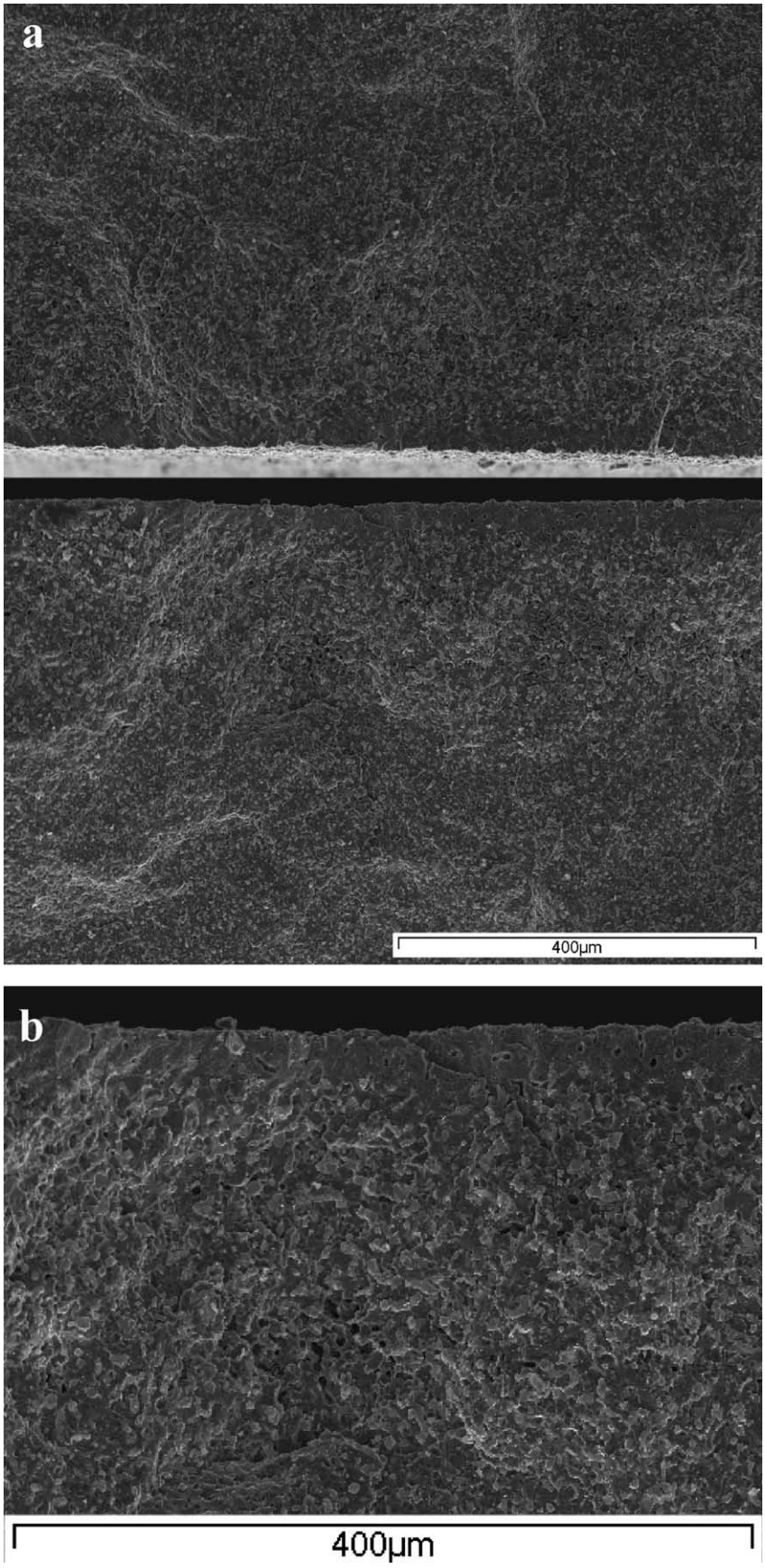

Fig. 8. Fracture surface (a) and origin of rupture (b) for a sample oxidised at 1300 °C for 100 h.

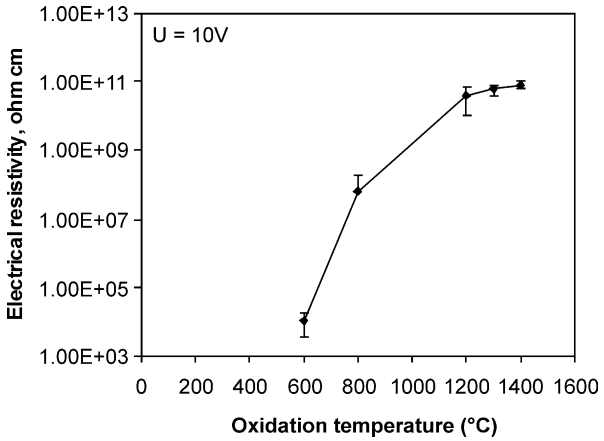

Fig. 9. Electrical resistivity of oxidised samples versus oxidation temperature.

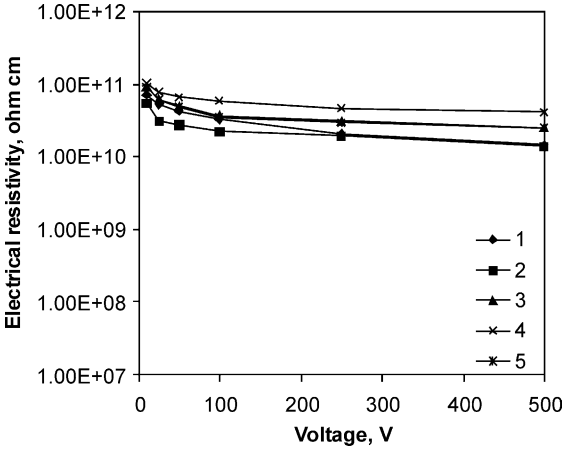

Fig. 10. Electrical resistivity of five bars oxidised at 1400 °C versus voltage applied during the measurements, showing the repetitivity of the resistivity measurements.

scale. Electrical resistivity measurements show that the application of this composite in oxidizing environment involves a strong decrease of the electrical conductivity due to surface modification. This has to be taken into account when the electrical properties of this material are of importance.

Acknowledgements

The work is supported by the European Project Research Training Network HPRN-CT-2000-00044 "Composite Corrosion". The research contract of K. Krnel is funded by the same Project. The authors wish to thank their colleagues: S. Guicciardi and C. Melandri for the measurement of mechanical properties and G. Fabbri for the evaluation of the electrical properties.

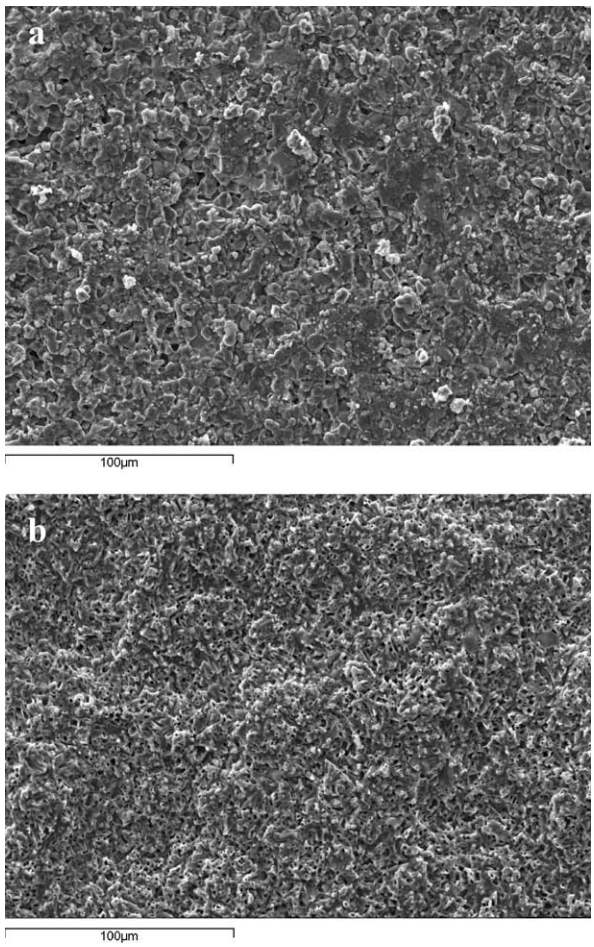

Fig. 11. SEM picture at lower magnification off oxidised surface at: (a) 800 °C, 100 h; (b) 1400 °C, 100 h.

References

1. Hale, D. K., The physical properties of composite materials. *J. Mater. Sci.*, 1976, **11**, 2105–2141.
2. Van de Goor, G., Sägesser, P. and Berroth, K., Electrically conductive ceramic composites. *Solid State Ionics*, 1997, **101–103**, 1163–1170.
3. Maruyama, T. and Yanagihara, K., High temperature oxidation and pesting of $Mo(Si,Al)_2$. *Mater. Sci. Eng.*, 1997, **A239–240**, 828–841.
4. Wei, W.-C. and Lee, J. S., Formation and reaction kinetics of Mo and Mo silicides in the preparation of $MoSi_2$/SiC Composites. *J. Eur. Ceram. Soc.*, 1998, **18**, 509–520.
5. Pan, J., Surappa, M. K., Saravan, R. A., Liu, B. W. and Yanf, D. M., Fabrication and characterisation of SiC/$MoSi_2$ composites. *Mater. Sci. Eng.*, 1998, **A244**, 191–198.
6. Newman, A., Sampath, S. and Herman, H., Processing and properties of $MoSi_2$–SiC and $MoSi_2$–Al_2O_3. *Mater. Sci. Eng.*, 1999, **A261**, 252–260.
7. Niihara, K. and Suzuki, Y., Strong monolithic and composite $MoSi_2$ materials by nanostructure design. *Mater. Sci. Eng.*, 1999, **A261**, 6–15.
8. Landon, M. and Thevenot, F., The AlN–SiC system: influence of elaboration routes on the solid solution formation and its mechanical properties. *Ceram. Int.*, 1991, **17**, 97–110.
9. Huang, J.-L. and Jih, J.-M., Investigation of SiC–AlN system:

part I. Microstructure and solid solution. *J. Mater. Res.*, 1995, **10**, 651–658.
10. Kurokawa, K., Houzumi, H., Saeki, I. and Takahashi, H., Low temperature oxidation of fully dense and porous $MoSi_2$. *Mater. Sci. Eng.*, 1999, **A261**, 292–299.
11. Bellosi, A., Landi, E. and Tampieri, A., Oxidation behaviour of aluminum nitride. *J. Mater. Res.*, 1993, **8**, 565–572.
12. Chen, J., Li, C., Fu, Z., Tu, X., Sundberg, M. and Pompe, R., Low temperature oxidation behavour of a $MoSi_2$-based material. *Mat. Sci. Eng.*, 1999, **A261**, 239–244.
13. Zhu, Y. T., Stan, M., Conzone, S. D. and Butt, D. P., Thermal oxidation kinetics of $MoSi_2$-based powders. *J. Am. Ceram. Soc.*, 1999, **82**, 2785–2790.
14. Zhu, Y. T. and Shu, L., Kinetics and products of molybdemun disilicide powder oxidation. *J. Am. Ceram. Soc.*, 2002, **85**, 507–509.
15. Natesan, K. and Deevi, S. C., Oxidation behaviour of molybdenum silicides and their composites. *Intermetallics*, 2000, **8**, 1147–1158.
16. Yanagihara, K., Maruyama, T. and Kazuhiro, N., Effect of third elements on the pesting suppresion of Mo–Si–X intermetallics (X = Al, Ta, Ti, Zr and Y). *Intermetallics*, 1996, **4**, S133–139.
17. Ramberg, C. E. and Worrell, W. L., Oxidation kinetics and composite scale formation in the system $Mo(Al,Si)_2$. *J. Am. Ceram. Soc.*, 2002, **85**, 444–452.
18. Lavrenko, V. A., Desmaison-Brut, M., Panasyuk, A. D. and Desmaison, J., Features of corrosion resistance of AlN–SiC ceramics in air up to 1600 °C. *J. Eur. Ceram. Soc.*, 1998, **18**, 2339–2343.
19. Li, J. F. and Watanabe, R., Pressureless sintering and high-temperature strength of SiC–AlN ceramics. *J. Ceram. Soc. Japan*, 1994, **102**(8), 727–731.
20. Stergiou, A., Tsakiropoulos, P. and Brown, A., The intermediate and high-temperature oxidation behaviour of Mo(Si1−xAlx)2 intermetallic alloys. *Intermetallics*, 1997, **96**, 69–81.
21. Ando, K., Chu, M.-C., Tsuji, K., Hirasawa, T., Kobayashi, Y. and Shigemi, S., Crack healing behaviour and high-temperature strength of mullite/SiC composite ceramics. *J. Eur. Ceram. Soc.*, 2002, **22**, 1313–1319.
22. Chaudhuri, S. P., Patra, S. K. and Chakraborty, A. K., Electrical resistivity of transition metal ion doped mullite. *J. Eur. Ceram. Soc.*, 1999, **19**, 2941–2950.